Creating virtual vertical radar profiles from surface reflection Ground Penetrating Radar data

Evert Slob, Jürg, Hunziker, Jan Thorbecke, and Kees Wapenaar
Department of Geoscience & Engineering, Delft University of Technology
Stevinweg 1, 2628 CN, Delft, The netherlands
e.c.slob@tudelft.nl, j.w.hunziker@tudelft.nl, j.w.thorbecke@tudelft.nl, c.p.a..wapenaar@tudelft.nl

***Abstract*—We present a three-dimensional scheme that can be used to compute a vertical radar profile from reflection data measured at the surface. This is done by first constructing a focusing wavefield, which focuses at the chosen location in the subsurface that is then the virtual receiver location for the vertical radar profile Green's function. Because the up- and downgoig parts of the Green's function are retrieved separately, these are very useful for imaging and inversion. We show with a numerical example that the method works well in a two-dimensional configuration.**

***Index Terms*—virtual source, virtual receiver, interferometry, autofocusing, 3D GPR.**

I. Introduction

For scalar acoustic waves it has been shown that a virtual receiver can be placed in the subsurface and the corresponding Green's function can be retrieved without having a physical source or receiver at that location and without the need to have a detailed model of the medium between the acquisition surface and the position of the virtual receiver [1], [2]. Creating vertical profile data has been performed before to improve interpretation [3], but this has been a model-driven method, which does need detailed information on the overburden.

Here we present a three-dimensional electromagnetic scheme similar to the acoustic schemes of [4], [5], but now for the general case of the vector electromagnetic wavefield. The electromagnetic scheme can be applied to a three-dimensional heterogeneous medium where the medium can be characterised by the electric permittivity and magnetic permeability values that vary smoothly in all directions. We assume that two horizontal components of the electric field are recorded on a horizontal planar surface. We formally split the recorded wavefield into up- and downgoing wavefields at the receiver level and at the focusing depth level. We then define a focusing wavefield that focuses at a particular location in the subsurface. Both the upgoing and downgoing parts of the focusing wavefield can be found from the measured reflection data and an estimate of the direct arrival from the surface source point to the subsurface focusing point. This leads to Green's function retrieval corresponding to a virtual vertical radar profile for any point in the subsurface. A 2D numerical example illustrates the Green's function retrieval scheme.

II. EM theory

The representations are derived in the frequency domain, but are valid in the time domain. To this end, we define the time-Fourier transform of a space-time dependent vector-quantity as $\hat{\boldsymbol{u}}(\boldsymbol{x},\omega) = \int_{t=0}^{\infty} \exp(-\mathrm{j}\omega t)\boldsymbol{u}(\boldsymbol{x},t)\mathrm{d}t$, where j is the imaginary unit, ω denotes angular frequency, and $\boldsymbol{x}$ is the position vector in three-dimensional space. In the space-frequency domain the electromagnetic field vector $\hat{\boldsymbol{u}}$ is given by $\hat{\boldsymbol{u}}^t(\boldsymbol{x},\omega) = (\hat{\boldsymbol{E}}^t(\boldsymbol{x},\omega), \hat{\boldsymbol{H}}^t(\boldsymbol{x},\omega))$, with $\hat{\boldsymbol{E}}(\boldsymbol{x},\omega)$ and $\hat{\boldsymbol{H}}(\boldsymbol{x},\omega)$ being the electric and magnetic field vectors and the superscript t denotes transposition.

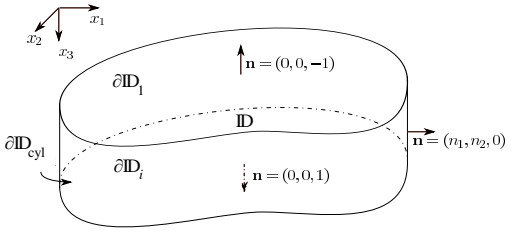

Fig. 1. Configuration for one-way reciprocity theorems.

Here we give the reciprocity relations pertaining to a specific domain in three-dimensional space, which is bounded by two planar surfaces that extend horizontally to infinity, see Figure 1. The domain $\mathbb{D}$ is bounded at the top by the boundary $\partial\mathbb{D}_1$ at depth level $x_{3;1}$, at the bottom by the boundary $\partial\mathbb{D}_i$ at depth level $x_{3;i}$, and at the side by a cylindrical boundary. Each boundary has a unique outward pointing unit normal vector $\boldsymbol{n}$. A reciprocity theorem in general interrelates two independent states, labeled A and B, in one and the same domain, but the fields, sources and the medium parameters in the two states need not be the same [6], [7]. The heterogeneities are not restricted to occur only inside the domain $\mathbb{D}$, but may extend over all space. In our derivations here we assume all medium parameters inside $\mathbb{D}$ to be the same in both states and we assume that all sources are outside the domain $\mathbb{D}$. The global form of the reciprocity theorem of the time-convolution type is given by [8]

$$\int_{\partial\mathbb{D}_1} (\hat{\boldsymbol{u}}_{1;A}^t \hat{\boldsymbol{u}}_{2;B} - \hat{\boldsymbol{u}}_{2;A}^t \hat{\boldsymbol{u}}_{1;B})\mathrm{d}^2\boldsymbol{x} = \int_{\partial\mathbb{D}_i} (\hat{\boldsymbol{u}}_{1;A}^t \hat{\boldsymbol{u}}_{2;B} - \hat{\boldsymbol{u}}_{2;A}^t \hat{\boldsymbol{u}}_{1;B})\mathrm{d}^2\boldsymbol{x}, \quad (1)$$

where the new vectors $\hat{\boldsymbol{u}}_1$ and $\hat{\boldsymbol{u}}_2$ contain horizontal components of the electric and magnetic fields given by $\hat{\boldsymbol{u}}_1 = (\hat{E}_1, \hat{E}_2)^t$ and $\hat{\boldsymbol{u}}_2 = (\hat{H}_2, -\hat{H}_1)^t$. For the reciprocity theorem

of the time-correlation type we will additionally assume that the medium inside $\mathbb{D}$ is lossless and then it is in global form given by [8]

$$\int_{\partial\mathbb{D}_1} (\hat{\boldsymbol{u}}^{\dagger}_{1;A}\hat{\boldsymbol{u}}_{2;B} + \hat{\boldsymbol{u}}^{\dagger}_{2;A}\hat{\boldsymbol{u}}_{1;B})\mathrm{d}^2\boldsymbol{x} = \int_{\partial\mathbb{D}_i} (\hat{\boldsymbol{u}}^{\dagger}_{1;A}\hat{\boldsymbol{u}}_{2;B} + \hat{\boldsymbol{u}}^{\dagger}_{2;A}\hat{\boldsymbol{u}}_{1;B})\mathrm{d}^2\boldsymbol{x}, \tag{2}$$

where the superscript † means complex conjugation and transposition. At either side of both depth levels of the planar boundaries of $\mathbb{D}$ we can write the horizontal components of the electric field as up- and downgoing wavefields according to

$$\hat{\boldsymbol{u}}_1 = \hat{\boldsymbol{u}}^{+}_1 + \hat{\boldsymbol{u}}^{-}_1, \tag{3}$$

where $\hat{\boldsymbol{u}}^{+}_1$ denotes the downgoing and $\hat{\boldsymbol{u}}^{-}_1$ denotes the upgoing electric field components. The horizontal components of the magnetic field vector can be written in terms of the up- and downgoing electric fields as [9]

$$\hat{\boldsymbol{u}}_2 = \hat{\boldsymbol{M}}^{-1}\partial_3(\hat{\boldsymbol{u}}^{+}_1 + \hat{\boldsymbol{u}}^{-}_1), \tag{4}$$

where the spatial derivatives with respect to coordinate x_k, with $k = 1, 2, 3$ are written as ∂_k and with the operator matrix $\hat{\boldsymbol{M}}$ given by

$$\hat{\boldsymbol{M}} = \begin{pmatrix} -\zeta + \partial_1\eta^{-1}\partial_1 & \partial_1\eta^{-1}\partial_2 \\ \partial_2\eta^{-1}\partial_1 & -\zeta + \partial_2\eta^{-1}\partial_2 \end{pmatrix}, \tag{5}$$

where $\eta = \mathrm{j}\omega\varepsilon$ and $\zeta = \mathrm{j}\omega\mu$. Notice that $\hat{\boldsymbol{M}}^t = \hat{\boldsymbol{M}}$. Following a procedure similar to the one given in Appendix C in [10] we assume that the permeability and permittivity at the depth levels $x_{3;1}$ and $x_{3;i}$ have zero vertical derivative and are continuously differentiable in horizontal direction, then we can rewrite equations (1) and (2) using equations (3) and (4) as

$$-\int_{\partial\mathbb{D}_1}\Big[(\hat{\boldsymbol{u}}^{+}_{1;A})^t\hat{\boldsymbol{M}}^{-1}\partial_3\hat{\boldsymbol{u}}^{-}_{1;B} + (\hat{\boldsymbol{u}}^{-}_{1;A})^t\hat{\boldsymbol{M}}^{-1}\partial_3\hat{\boldsymbol{u}}^{+}_{1;B}\Big]\,\mathrm{d}^2\boldsymbol{x} = \int_{\partial\mathbb{D}_i}\Big[(\hat{\boldsymbol{M}}^{-1}\partial_3\hat{\boldsymbol{u}}^{-}_{1;A})^t\hat{\boldsymbol{u}}^{+}_{1;B} + (\hat{\boldsymbol{M}}^{-1}\partial_3\hat{\boldsymbol{u}}^{+}_{1;A})^t\hat{\boldsymbol{u}}^{-}_{1;B}\Big]\,\mathrm{d}^2\boldsymbol{x}, \tag{6}$$

and

$$-\int_{\partial\mathbb{D}_1}\Big[(\hat{\boldsymbol{u}}^{+}_{1;A})^{\dagger}\hat{\boldsymbol{M}}^{-1}\partial_3\hat{\boldsymbol{u}}^{+}_{1;B} + (\hat{\boldsymbol{u}}^{+}_{1;A})^{\dagger}\hat{\boldsymbol{M}}^{-1}\partial_3\hat{\boldsymbol{u}}^{+}_{1;B}\Big]\,\mathrm{d}^2\boldsymbol{x} = \int_{\partial\mathbb{D}_i}\Big[(\hat{\boldsymbol{M}}^{-1}\partial_3\hat{\boldsymbol{u}}^{+}_{1;A})^{\dagger}\hat{\boldsymbol{u}}^{+}_{1;B} + (\hat{\boldsymbol{M}}^{-1}\partial_3\hat{\boldsymbol{u}}^{+}_{1;A})^{\dagger}\hat{\boldsymbol{u}}^{+}_{1;B}\Big]\,\mathrm{d}^2\boldsymbol{x}. \tag{7}$$

In equation (7) an additional approximation is made by ignoring evanescent waves at depth levels $x_{3;1}$ and $x_{3;i}$.

III. Green's function representations for vertical radar profile

Since it is our goal to retrieve the vertical radar profile from the reflection response measured at the surface we derive here Green's function representations for vertical radar profiles in terms of the surface reflection response. We use equations (6) and (7) and define the two states as follows. State A is chosen as a focusing electric wavefield in the medium that in $\mathbb{D}$ is the same as the actual medium in which the measurements are carried out, but that is reflection-free outside $\mathbb{D}$. It has a downgoing wavefield above depth level $x_{3;1}$ such that it focuses at depth level $x_{3;i}$. Since we work with vector fields we introduce two realisations and for each realisation we have the two horizontal electric field components in the vector $\hat{\boldsymbol{u}}_1$. Hence, at depth level $x_{3;1}$ the electric field in state A is a focusing field given by

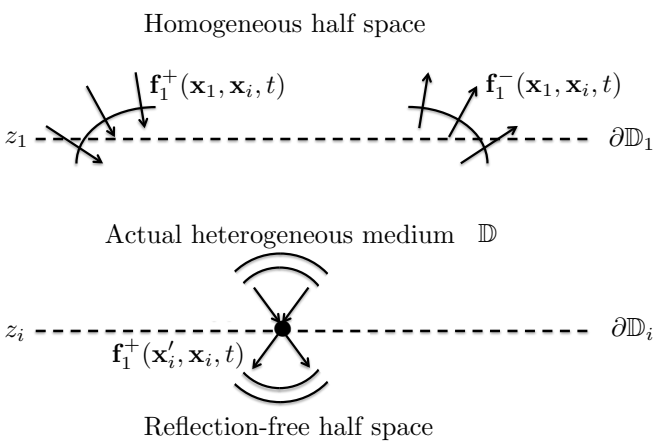

Fig. 2. The focusing wavefield $\boldsymbol{f}^{\pm}_1$ at the different depth levels.

$$\hat{\boldsymbol{u}}^{\pm}_{1;A}(\boldsymbol{x}_1, \omega) = \hat{\boldsymbol{f}}^{\pm}_1(\boldsymbol{x}_1, \boldsymbol{x}'_i, \omega), \tag{8}$$

where $\hat{\boldsymbol{f}}^{+}_1$ is a 2×2 downgoing wavefield matrix and the first argument denotes that $\boldsymbol{x}_1$ is a point at the receiver level and the second argument $\boldsymbol{x}'_i$ is a point at the focusing level. The focusing condition at depth level $x_{3;i}$ is given as

$$\partial_3\hat{\boldsymbol{u}}^{+}_{1;A}(\boldsymbol{x}_i, \omega) = -\frac{1}{2}\hat{\boldsymbol{M}}(\boldsymbol{x}_H, \omega)\delta(\boldsymbol{x}_H - \boldsymbol{x}'_H), \tag{9}$$

where $\boldsymbol{x}_H$ demotes the horizontal components of the position vector $\boldsymbol{x}$ and the focusing condition states that the electric wavefield focuses at $\boldsymbol{x}_i = \boldsymbol{x}'_i$, see Figure 2. For depth levels $x_3 > x_{3;i}$ the wavefield propagates down and no upward traveling wavefield exists, hence $\partial_3\hat{\boldsymbol{u}}^{-}_{1;A}(\boldsymbol{x}_i, \omega) = \boldsymbol{0}$, where $\boldsymbol{0}$ is the 2×2 zero matrix.

For state B we choose the actual state of the measurement and we assume two sources are used separately yielding again a 2×2 matrix for the electric field. We assume the source wavefield is located at depth level $x_{3;1}$ and the field can then be written as

$$\partial_3\hat{\boldsymbol{u}}^{+}_{1;B}(\boldsymbol{x}_1, \omega) = -\frac{1}{2}\hat{\boldsymbol{M}}(\boldsymbol{x}_H, \omega)\delta(\boldsymbol{x}_H - \boldsymbol{x}'_H), \tag{10}$$

$$\partial_3\hat{\boldsymbol{u}}^{-}_{1;B}(\boldsymbol{x}_1, \omega) = \frac{1}{2}\hat{\boldsymbol{M}}(\boldsymbol{x}_H, \omega)\hat{\boldsymbol{R}}(\boldsymbol{x}_1, \boldsymbol{x}'_1, \omega), \tag{11}$$

where $\hat{\boldsymbol{R}}(\boldsymbol{x}_1, \boldsymbol{x}'_1, \omega)$ denotes the 2×2 matrix electric field earth reflection response measured at $\boldsymbol{x}_1$ generated by a source at $\boldsymbol{x}'_1$. At depth level $x_{3;i}$ the electric field is the desired Green's

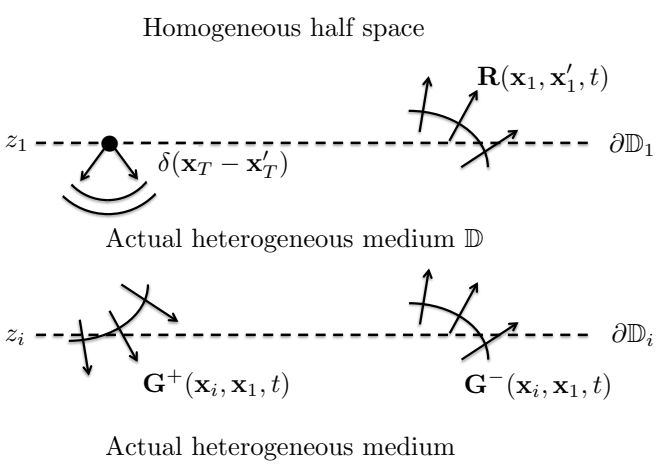

Fig. 3. The actual wavefield consists of a downgoing source wavefield and its corresponding reflection response $\boldsymbol{R}$ at the depth level $x_{3;1}$ and the up- and downgoing parts of the Green's function at depth level $x_{3;i}$.

function for a receiver located at level $x_{3;i}$ and generated by the source at $\boldsymbol{x}'_1$. It is given by

$$\hat{\boldsymbol{u}}^{\pm}_{1;B}(\boldsymbol{x}_i, \omega) = \hat{\boldsymbol{G}}^{\pm}(\boldsymbol{x}_i, \boldsymbol{x}'_1, \omega), \tag{12}$$

see Figure 3.

Substituting these wavefields in equations (6) and (7) yields

$$\int_{\partial\mathbb{D}_1} [\hat{\boldsymbol{f}}^+_1(\boldsymbol{x}'_1, \boldsymbol{x}_i, \omega)]^t \hat{\boldsymbol{R}}(\boldsymbol{x}'_1, \boldsymbol{x}_1, \omega) \mathrm{d}\boldsymbol{x}'_H - [\hat{\boldsymbol{f}}^-_1(\boldsymbol{x}_1, \boldsymbol{x}_i, \omega)]^t = \hat{\boldsymbol{G}}^-(\boldsymbol{x}_i, \boldsymbol{x}_1, \omega), \tag{13}$$

$$-\int_{\partial\mathbb{D}_1} [\hat{\boldsymbol{f}}^-_1(\boldsymbol{x}'_1, \boldsymbol{x}_i, \omega)]^\dagger \hat{\boldsymbol{R}}(\boldsymbol{x}'_1, \boldsymbol{x}_1, \omega) \mathrm{d}\boldsymbol{x}'_H + [\hat{\boldsymbol{f}}^+_1(\boldsymbol{x}_1, \boldsymbol{x}_i, \omega)]^\dagger = \hat{\boldsymbol{G}}^+(\boldsymbol{x}_i, \boldsymbol{x}_1, \omega), \tag{14}$$

where we dropped the primes on $\boldsymbol{x}_i$, and interchanged them for $\boldsymbol{x}_1$ such that now the integration variable is primed. Equations (13) and (14) represent the upgoing and downgoing electric field at a receiver location $\boldsymbol{x}_i$, generated by an electric source at $\boldsymbol{x}_1$, in terms of the measured electric reflection response and the up- and downgoing focusing wavefield $\hat{\boldsymbol{f}}^{\pm}_1$ that focuses at the receiver point $\boldsymbol{x}_i$. At this point both the focusing wavefield and the vertical radar profile Green's functions are unknown. In the nest section we show how the focusing wavefield can be retrieved from the reflection response, after which the Green's functions can be computed.

IV. Green's function retrieval

As outlined in [4], [5] for scalar wavefileds these coupled equations in the time domain can be evaluated in a time-window where the focusing wavefield is non-zero while the Green's function is. The time domain Green's function $\boldsymbol{G}(\boldsymbol{x}_i, \boldsymbol{x}_1, t)$ has a first arrival that can be received at $\boldsymbol{x}_i$ when the wavefield is generated at $\boldsymbol{x}_1$ at time instant $t_d(\boldsymbol{x}_i, \boldsymbol{x}_1)$, which is the smallest time for the wavefeld to travel through $\mathbb{D}$ and arrive at $\boldsymbol{x}_i$. Hence for $t < t_d(\boldsymbol{x}_i, \boldsymbol{x}_1)$ $\boldsymbol{G}(\boldsymbol{x}_i, \boldsymbol{x}_1, t) = \boldsymbol{0}$. The focusing functions are non-zero on the interval $-t_d(\boldsymbol{x}_i, \boldsymbol{x}_1) < t < t_d(\boldsymbol{x}_i, \boldsymbol{x}_1)$ and we can evaluate the time domain equivalents of equations (13) and (14) in this interval as

$$\int_{\partial\mathbb{D}_1} \int_{-t_d(\boldsymbol{x}_i, \boldsymbol{x}'_1)}^{t} [\boldsymbol{f}^+_1(\boldsymbol{x}'_1, \boldsymbol{x}_i, t')]^t \boldsymbol{R}(\boldsymbol{x}'_1, \boldsymbol{x}_1, t - t') \mathrm{d}t' \mathrm{d}^2\boldsymbol{x}'_H = [\boldsymbol{f}^-_1(\boldsymbol{x}_1, \boldsymbol{x}_i, t)]^t \tag{15}$$

$$\int_{\partial\mathbb{D}_1} \int_{-t_d(\boldsymbol{x}_i, \boldsymbol{x}'_1)}^{t} [\boldsymbol{f}^-_1(\boldsymbol{x}'_1, \boldsymbol{x}_i, -t')]^t \boldsymbol{R}(\boldsymbol{x}'_1, \boldsymbol{x}_1, t - t') \mathrm{d}t' \mathrm{d}^2\boldsymbol{x}'_H = [\boldsymbol{f}^+_1(\boldsymbol{x}_1, \boldsymbol{x}_i, -t)]^t. \tag{16}$$

We observe here that the time instant $t = t_d(\boldsymbol{x}_i, \boldsymbol{x}'_1)$ is necessary to evaluate the integrals. The upgoing part of the focusing wavefield is zero at this instant but the downgoing field is not. The downgoing focusing wavefield at the boundary $\partial\mathbb{D}_1$ is the inverse of the transmission response because that is the wavefield that will produce a focus at the boundary $\partial\mathbb{D}_i$. Let us denote this wavefield as $\boldsymbol{T}^{-1}_d(\boldsymbol{x}_i, \boldsymbol{x}_1, t)$ and split the downgoing focusing wavefield up in a direct part and a coda given by

$$\boldsymbol{f}^+_1(\boldsymbol{x}_1, \boldsymbol{x}_i, t) = \boldsymbol{T}^{-1}_d(\boldsymbol{x}_i, \boldsymbol{x}_1, t) + \boldsymbol{f}^+_{1;c}(\boldsymbol{x}_1, \boldsymbol{x}_i, t), \tag{17}$$

where $\boldsymbol{f}^+_{1;c}(\boldsymbol{x}_1, \boldsymbol{x}_i, t) = \boldsymbol{0}$ for $|t| \geq t_d(\boldsymbol{x}_i, \boldsymbol{x}_1)$ and denotes the coda of the downgoing wavefield. With this definition equations (15) and (16) are rewritten as

$$\int_{\partial\mathbb{D}_1} \int_{-t_d(\boldsymbol{x}_i, \boldsymbol{x}'_1)}^{t} [\boldsymbol{f}^+_{1;c}(\boldsymbol{x}'_1, \boldsymbol{x}_i, t')]^t \boldsymbol{R}(\boldsymbol{x}'_1, \boldsymbol{x}_1, t - t') \mathrm{d}t' \mathrm{d}^2\boldsymbol{x}'_H + [\boldsymbol{f}^-_{1;0}(\boldsymbol{x}_1, \boldsymbol{x}_i, t)]^t = [\boldsymbol{f}^-_1(\boldsymbol{x}_1, \boldsymbol{x}_i, t)]^t, \tag{18}$$

$$\int_{\partial\mathbb{D}_1} \int_{-t_d(\boldsymbol{x}_i, \boldsymbol{x}'_1)}^{t} [\boldsymbol{f}^-_1(\boldsymbol{x}'_1, \boldsymbol{x}_i, -t')]^t \boldsymbol{R}(\boldsymbol{x}'_1, \boldsymbol{x}_1, t - t') \mathrm{d}t' \mathrm{d}^2\boldsymbol{x}'_H = [\boldsymbol{f}^+_{1;c}(\boldsymbol{x}_1, \boldsymbol{x}_i, -t)]^t, \tag{19}$$

where

$$[\boldsymbol{f}^-_{1;0}(\boldsymbol{x}_1, \boldsymbol{x}_i, t)]^t = \int_{\partial\mathbb{D}_1} \int_{-t_d(\boldsymbol{x}_i, \boldsymbol{x}'_1)}^{t} [\boldsymbol{T}^{-1}_d(\boldsymbol{x}_i, \boldsymbol{x}'_1, t')]^t \boldsymbol{R}(\boldsymbol{x}'_1, \boldsymbol{x}_1, t - t') \mathrm{d}t' \mathrm{d}^2\boldsymbol{x}'_H. \tag{20}$$

Equations (18) and (19) are two coupled Marchenko type equations that can be solved for the up- and downgoing focusing wavefield from the measured surface reflection response and an estimate of the inverse of the direct arrival from the surface to the focus point [5]. Once the focusing functions have been computed, equations (13) and (14) can be used to obtain the up-and downgoing parts of the Green's function. In the next section we give a two-dimensional example.

V. Numerical example

To demonstrate the effectiveness of the method in computing the focusing and subsequently retrieving the Green's functions we have performed a two-dimensional modelling test. The model is shown in Figure 4 and has vertical and lateral variations in ε. The model size is 40 m in length and 6 m in depth. We have used 501 sources and receivers

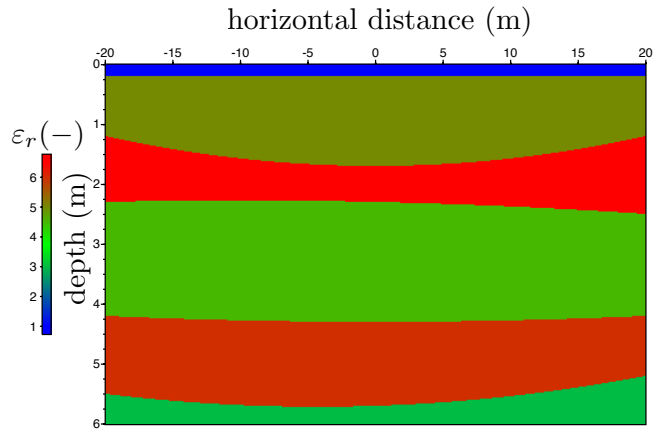

Fig. 4. The 2D model with relative values of the epsilon distribution.

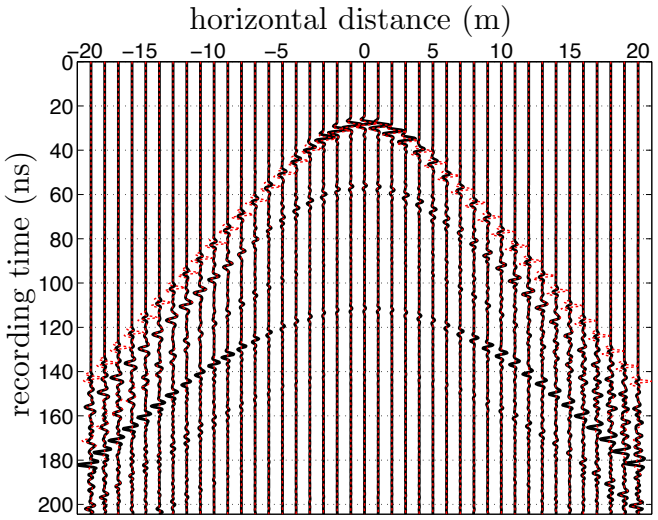

Fig. 5. The retrieved Green's function (red dashed lines) over the directly modeled Green's function (black solid lines).

equally spaced 10 cm above the first reflector. The data was modeled using an FDTD code and a Ricker wavelet with center frequency of 250 MHz was used. Equations (18) and (19) were solved using a smoothed background model to compute the space-time curves to determine the window in which to solve for the focusing functions for a receiver point at 3.9 m below the source level. Then we computed the Green's function and we show results for a receiver in the center for all sources along the original source line.

The retrieved Green's function is shown in red dashed lines on top of the direct modeled Green's function shown in black solid lines in Figure 5. It can be seen that for small offsets the Green's function is reasonably well retrieved. The first reflection has some amplitude errors even at small offsets, but the errors become quite large for large offsets. The reason is that the spectral bandwidth of the measured data is restricted due to the fact that both sources and receivers are in the air, which has the highest velocity in the model. The first and second layers below the air have the highest values for the electric permittivity and this reduces the spectral bandwidth of the recorded data. It can also be observed that the second to fourth events are quite well retrieved up to large offsets. This is because they are the reflection from the bottom of the fourth layer, which is a low-velocity layer, and multiple reflections which have a reduced spectral bandwidth.

VI. Conclusion

We have shown the theory and a numerical example to retrieve the Green's function of a virtual receiver located at a chosen position in the subsurface and a source at the original receiver plane without needing detailed information about the medium between the surface and virtual receiver level. The example shows that the theory works well within the spectral bandwidth of the measured data. Effects of noise, errors in the estimate of the first arrival, and losses in the subsurface remain to be investigated.

Acknowledgment

This research has been performed in the framework of the Active and Passive Microwaves for Security and Subsurface imaging (AMISS) EU 7th Framework Marie Curie Actions IRSES project (PIRSES-GA-2010-269157). This abstract is part of the research program of the Netherlands research center for Integrated Solid Earth Science.

References

[1] F. Broggini, R. Snieder, and K. Wapenaar, "Focusing the wavefield inside an unknown 1D medium: Beyond seismic interferometry," *Geophysics*, vol. 77, no. 5, pp. A25–A28, September-October 2012.

[2] K. Wapenaar, F. Broggini, E. Slob, and R. Snieder, "Three-dimensional single-sided marchenko inverse scattering, data-driven focusing, green's function retrieval, and their mutual relations," *Physical Review Letters*, vol. 110, p. 084301, Feb 2013. [Online]. Available: http://link.aps.org/doi/10.1103/PhysRevLett.110.084301

[3] R. Alá'i and C. P. A. Wapenaar, "Pseudo VSP generation from surface measurements: A new tool for seismic interpretation," *Journal of Seismic Exploration*, vol. 3, pp. 79–94, 1994.

[4] E. Slob, K. Wapenaar, F. Broggini, and R. Snieder, "Seismic reflector imaging while eliminating internal multiples using Marchenko-type equations," *Geophysics*, vol. 79, no. 2, pp. S63–S76, March-April 2014.

[5] K. Wapenaar, J. Thorbecke, J. van der Neut, F. Broggini, E. Slob, and R. Snieder, "Marchenko Imaging," *Geophysics*, vol. 79, no. 3, pp. WA39–WA57, May-June 2014.

[6] B. Ru-Shao Cheo, "A reciprocity theorem for electromagnetic fields with general time dependence," *IEEE Trans. Ant. Prop.*, vol. 13, pp. 278–284, 1965.

[7] N. Bojarski, "Generalized reaction principles and reciprocity theorems for the wave equations, and the relationships between time-advanced and time-retarded fields." *Journal of the Acoustical Society of America*, vol. 74, pp. 281–285, 1983.

[8] K. Wapenaar and J. Fokkema, "Reciprocity theorems for diffusion, flow and waves," *A.S.M.E. Journal of Applied Mechanics*, vol. 71, no. 1, pp. 145–150, 2004.

[9] E. Slob, "Interferometry by deconvolution of multi-component multi-offset GPR data," *IEEE Trans. Geoscience and Remote Sensing*, vol. 47, no. 3, pp. 828–838, March 2009.

[10] C. P. A. Wapenaar and A. J. Berkhout, *Elastic wave field extrapolation: Redatuming of single- and multi- component seismic data*, ser. Advances in Exploration Geophysics. Elsevier Science Publishers, 1989.

[11] K. Wapenaar, F. Broggini, and R. Snieder, "Creating a virtual source inside a medium from reflection data: heuristic derivation and stationary-phase analysis," *Geophysical Journal International*, vol. 190, no. 2, pp. 1020–1024, AUG 2012.